

Noise, gain, and capture probability of p-type InAs-GaAs quantum-dot and quantum dot-in-well infrared photodetectors

Seyoum Wolde, Yan-Feng Lao, A. G. Unil Perera, Y. H. Zhang, T. M. Wang, J. O. Kim, Ted Schuler-Sandy, Zhao-Bing Tian, and S. Krishna

Citation: *Journal of Applied Physics* **121**, 244501 (2017); doi: 10.1063/1.4989834

View online: <http://dx.doi.org/10.1063/1.4989834>

View Table of Contents: <http://aip.scitation.org/toc/jap/121/24>

Published by the *American Institute of Physics*

AIP | Journal of
Applied Physics

Save your money for your research.
It's now **FREE** to publish with us -
no page, color or publication charges apply.

Publish your research in the
Journal of Applied Physics
to claim your place in applied
physics history.

Noise, gain, and capture probability of p-type InAs-GaAs quantum-dot and quantum dot-in-well infrared photodetectors

Seyoum Wolde,¹ Yan-Feng Lao,^{1,a)} A. G. Unil Perera,^{1,b)} Y. H. Zhang,² T. M. Wang,² J. O. Kim,³ Ted Schuler-Sandy,³ Zhao-Bing Tian,³ and S. Krishna^{3,c)}

¹Department of Physics and Astronomy, Georgia State University, Atlanta, Georgia 30303, USA

²Key Laboratory of Artificial Structures and Quantum Control, Department of Physics and Astronomy, Shanghai Jiao Tong University, Shanghai 200240, China

³Center for High Technology Materials, Department of Electrical and Computer Engineering, University of New Mexico, Albuquerque, New Mexico 87106, USA

(Received 27 January 2017; accepted 11 June 2017; published online 27 June 2017)

We report experimental results showing how the noise in a Quantum-Dot Infrared photodetector (QDIP) and Quantum Dot-in-a-well (DWELL) varies with the electric field and temperature. At lower temperatures (below ~ 100 K), the noise current of both types of detectors is dominated by generation-recombination (G-R) noise which is consistent with a mechanism of fluctuations driven by the electric field and thermal noise. The noise gain, capture probability, and carrier life time for bound-to-continuum or quasi-bound transitions in DWELL and QDIP structures are discussed. The capture probability of DWELL is found to be more than two times higher than the corresponding QDIP. Based on the analysis, structural parameters such as the numbers of active layers, the surface density of QDs, and the carrier capture or relaxation rate, type of material, and electric field are some of the optimization parameters identified to improve the gain of devices. *Published by AIP Publishing.* [<http://dx.doi.org/10.1063/1.4989834>]

I. INTRODUCTION

Quantum dot (QD) and quantum dot-in-a-well (DWELL) infrared photodetectors have attracted a lot of attention due to the sensitivity to normally incident radiation which is hardly possible without optical coupling in quantum well infrared photodetector (QWIP) and for multiple band detections in the infrared (IR).^{1,2} In QD structures, the detection mechanism is based on the intersubband photoexcitation of the charge carriers from confined states in the dots to the continuum or quasi-bound states. In bulk semiconductors, such as *p*-doped ($1 \times 10^{19} \text{ cm}^{-3}$) GaAs, the relaxation time is very short ~ 0.1 ps, while QDs and DWELLs have longer carrier lifetimes (up to nanoseconds),³⁻⁵ which leads to efficient collection of photo-excited carriers and ultimately leads to higher photoconductive gain^{4,5} and higher operating temperatures.⁶ The optical nonlinearities and the gain dynamics in the QD-based devices are dependent on the carriers' emission-capture dynamics of the QDs.⁵ Hence, the capture probability and relaxation mechanisms of carriers in QDs deserve further research for the improvement of the performance of the QD-based devices.

The fundamental noise components, shot noise (G-R) and thermal noise, are frequency independent. The analysis of G-R and thermal noises which change with bias voltage and temperature helps to understand carrier transport and emission/capture mechanisms such as capture probability

which is critical in determining the responsivity of devices. To realize high-performance (higher quantum efficiency, responsivity, and detectivity) devices, the noise power spectral density, carrier lifetime, and photoconductive and dark current gain are the most important parameters that need to be better understood and optimized. The *p*-type InAs/GaAs QD structures discussed here are based on holes as charge carriers instead of electrons. The energy levels (or density of states) of holes in a QD are much more closely spaced than those of electrons due to larger effective mass of holes. The hole-capture dynamics in QD-based structures is important for future information processing and storage devices.⁷ Thus, we report comparisons between *p*-type Quantum-Dot Infrared photodetector (QDIP) and DWELL's dark current gain and capture probabilities, using directly measured noise power spectral density and dark current.

In a highly *p*-doped QD structures, photoexcited holes can undergo several processes. First, the holes can relax back into the ground state of the QD. A unipolar nature of QDIP device greatly reduced electron-hole scattering. Photoexcited carriers have longer lifetime due to reduced hole-phonon scattering because of the phonon bottleneck.⁴ The dominant hole-hole scattering process is usually not a very fast process. Therefore, the photoexcited holes that escape from the QD driven by electric field either relax into a different quantum dot or will be collected at the contact. Hence, the effective carrier life time, the capture probability, and the number of quantum dot layers are very important parameters in determining the gain and responsivity of the device.

When the carrier is excited from the QD, the time photoexcited carrier takes before relaxing back into the QD state is the effective carrier life time. Depending upon the QD structure, the material, applied bias, and temperature, high

^{a)}Present address: Archcom Technology, Inc., South Plainfield, New Jersey 07080, USA. Electronic mail: ylao95@gmail.com

^{b)}Author to whom correspondence should be addressed: uperera@phy-astr.gsu.edu

^{c)}Present address: Department of Electrical and Computer Engineering, The Ohio State University, Columbus, Ohio 43210, USA. Electronic mail: krishna.53@osu.edu

values of photoconductive gains of n-type QDIPs have been reported,^{8–11} with the gain values varying from ~ 1 to $\sim 10^6$. High electron mobility in the barrier materials,⁸ the low carrier capture probability or long carrier life time,¹¹ and avalanche mechanisms^{9,10} are some of the mechanisms proposed for the large measured gain values. There are many gain measurements for n-type QDIPs, while very few attempts, such as p-type GaAs/AlGaAs QWIP¹² and Ge/Si QDIP,¹³ have been made so far to study the gain experimentally for p-type detectors. In this article, we present a study of the noise, noise gain, and capture probability of holes in highly p-doped InAs QD-based DWELL and QDIP. The capture probability of holes in DWELL is found to be about two times higher than the corresponding QDIP.

II. DEVICE STRUCTURES AND EXPERIMENTAL PROCEDURES

The detectors were grown by molecular beam epitaxy (MBE), consisting of 10 stacks of quantum dot and dot-in-a-well structures sandwiched between two highly doped p^+ -GaAs contact layers, grown on a semi-insulating GaAs substrate. The only difference between QDIP and DWELL is that in DWELL, the InAs QDs are placed in a 6 nm thick $\text{In}_{0.15}\text{Ga}_{0.85}\text{As}$ QW which in turn is surrounded by GaAs barrier layers. The dot density is about $5 \times 10^{10} \text{ cm}^{-2}$. A δ -doping technique is used with a sheet density of $5 \times 10^{11} \text{ cm}^{-2}$ p -type Be-dopants placed above the 13 nm thick GaAs spacer which introduces about 10 free holes in each QD. The QD layers are separated by thick ($\sim 80 \text{ nm}$) GaAs barriers to suppress the tunneling emissions between adjacent layers. The QDs have nearly pyramidal shape with the average base widths of $\sim 20\text{--}25 \text{ nm}$ and height of $\sim 5 \text{ nm}$. The devices were fabricated into square mesas of $400 \times 400 \mu\text{m}^2$ with an optical window of $260 \times 260 \mu\text{m}^2$ which allows front-side illumination. Other details of both devices are given in Lao *et al.*^{14,15}

To characterize the device, the square mesas and the ohmic contacts on the top and bottom layers were fabricated using standard wet chemical etching. Then the device was mounted on the cold head of the liquid nitrogen-cooled dewar and liquid helium-cooled cryostat to allow measurements of noise power spectral density and dark current. The voltage and current noise spectra were then amplified using a Stanford Research System, SR560 low-noise voltage amplifier with a fixed gain of $G = 1000$ and an SR 570 low-noise current preamplifier, respectively, and measured using an HP SRS-SR785 fast Fourier transform spectrum analyzer.

The p-type In(Ga)As/GaAs QDIP and DWELL are based on valence-band intersublevel hole transitions as opposed to conventional electron transitions. Two response bands observed at $\sim 1.5\text{--}3$ and $\sim 3\text{--}10 \mu\text{m}$ are due to transitions from the heavy-hole to spin-orbit split-off QD level and from the heavy-hole to heavy-hole level, respectively. The dominant bound to continuum (heavy hole (hh) to hh) transitions are indicated by arrows in Fig. 1(a). At 78 K, both QDIP and DWELL display promising results, such as a specific detectivity of $\sim 1.8 \times 10^9$ jones and maximum quantum efficiency of 17% and 9%, respectively, without employing

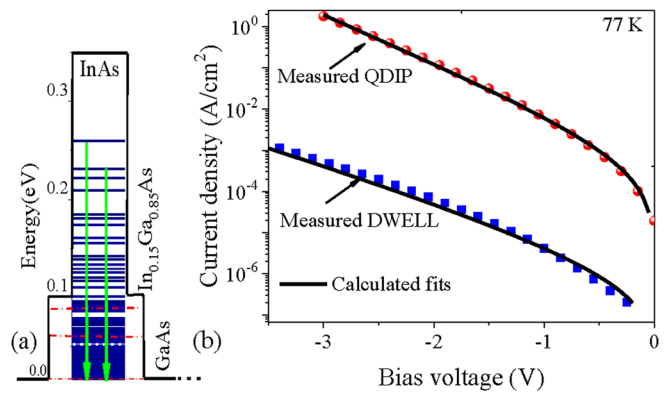


FIG. 1. (a) The valence band structure of DWELL without the spin orbit split off band. The dominant bound to continuum [heavy hole (hh) to hh] transitions are indicated by arrows. The only difference between DWELL and QDIP (not shown here) is that, in DWELL, the InAs QDs are placed in 6 nm thick $\text{In}_{0.15}\text{Ga}_{0.85}\text{As}$ QW which in turn is surrounded by GaAs barriers while in QDIP, the InAs QDs are directly sandwiched in the GaAs barriers. (b) Dark current density of DWELL (blue filled square) and QDIP (red filled circle) at 77 K. The solid lines are the corresponding calculated fits.

optimized structures, such as the dark current blocking layers. In order to compare between QD-based and other heterostructures, a 30 period of 18.8 nm p-doped GaAs emitter and 60 nm $\text{Al}_{0.28}\text{Ga}_{0.72}\text{As}$ barrier heterostructures¹⁶ were measured. Both QDIP (and DWELL) and GaAs/ $\text{Al}_{0.28}\text{Ga}_{0.72}\text{As}$ display nearly the same response wavelength range from $\sim 2\text{--}10 \mu\text{m}$.

III. RESULTS AND DISCUSSION

A. Dark current and noise power spectral density

An important property that brings about noise and a degradation of device sensitivity is the dark current. Hence, insight to noise begins with the analysis of dark current. Thermalized carrier transition from bound state in the QD to quasi-bound or continuum state contributes to the formation of dark current, and thus, the dark current density can be estimated as¹⁷

$$\langle J_d \rangle = 2ev \left(\frac{m^* kT}{2\pi\hbar^2} \right)^{3/2} \exp\left(-\frac{E_a}{kT}\right), \quad (1)$$

where e is the electronic charge, v is the drift velocity of holes, k is the Boltzmann constant, T is the temperature, \hbar is the reduced Planck constant, and E_a is the activation energy, and the transport effective mass m^* of holes can be written as¹⁸

$$m^* = \left(\frac{m_{lh}^{3/2} + m_{hh}^{3/2}}{m_{lh} + m_{hh}} \right)^2. \quad (2)$$

The activation energy depends on the total energy of hole transport,^{19,20} and it can be calculated as

$$E_a = E_0 - \beta F, \quad (3)$$

where F is the applied electric field intensity, E_0 is the activation energy at zero bias ($F = 0 \text{ kV/cm}$), and β is a scaling parameter in the presence of the electric field. The drift

velocity is essentially dependent on the electric field²¹ and can be expressed as

$$v = \mu F \left(1 + \left(\frac{\mu F}{v_s} \right)^2 \right)^{-1/2}, \quad (4)$$

where v_s is the saturation velocity of holes and μ is the mobility of holes. Substituting Eqs. (3) and (4) into Eq. (1) yields

$$\langle J_d \rangle = 2e\mu F \left(1 + \left(\frac{\mu F}{v_s} \right)^2 \right)^{-1/2} \left(\frac{m^* kT}{2\pi\hbar^2} \right)^{3/2} \exp\left(-\frac{E_0 - \beta F}{kT} \right) \quad (5)$$

Equation (5) is fitted to the experimentally measured dark current density for DWELL and QDIP at 77 K as shown in Fig. 1(b). The fitting parameters of dark current density for DWELL and QDIP at 77 K are given in Table I. The values of mobility are in the range of hole mobility in InAs.²² The saturation velocities are also within the range of saturation velocities of holes for InAs or GaAs.²³ The activation energy obtained from Arrhenius data is $E_0 = 0.254$ eV.

At low temperature, the intersubband detectors like QDIP and DWELL usually show no $1/f$ noise contribution due to the unipolar nature of devices and the maturity of III-V technology.²⁴ Hence, the two major noise contributions are Johnson noise and shot or generation-recombination (G-R) noise. Johnson noise is caused by the random thermal motion of charge carriers, and the Johnson noise current I_{th} in terms of bias voltage V can be expressed as

$$I_{th}^2 = \frac{4kT\Delta f}{R}, \quad (6)$$

where $R = \frac{dV}{dI_d}$, I_d is the dark current, T is the temperature in degree kelvin, and Δf is the bandwidth. The excited carrier from the QD levels below the Fermi level can escape to the quasi-bound levels near the continuum, and then tunnel or thermally escape out of the QD; then travel either to the contact or get trapped in another QDs or in shallow barrier state, normally a wetting layer state, from which the carrier can easily escape again. The trapping can also take place in the excited states of the QD from which the carrier escaped and recombine into the lower QD levels. These emission and captures are the main cause of fluctuating number of mobile carriers (or G-R noise) in the dot and well structures where the noise current is related to gain g via the general theoretical description given by Beck²⁵ as

$$I_{g-r}^2 = 4eg \left(1 - \frac{p_c}{2} \right) I_d \Delta f, \quad (7)$$

TABLE I. Fitting parameters for dark current density at 77 K for DWELL and QDIP structures in the negative bias region.

	DWELL	QDIP
μ (cm ² /V s)	245	253
v_s (10 ⁶ cm/s)	1.53	2.36
β (10 ⁻²⁷ m C)	1.70	2.71

where p_c is the capture probability of carriers, and for N period, the photoconductive gain is given by $g = 1/Np_c$. Assuming that G-R noise and Johnson noise are statistically independent, the total measured white noise power spectral density $S_I(f)$ of photodetector is given by $S_I(f) = I_{g-r}^2 + I_{th}^2$. Hence, Eq. (7) yields

$$g = \frac{I_{g-r}^2}{4eI_d\Delta f} + \frac{1}{2N}. \quad (8)$$

The low-frequency current noise power spectral density is usually estimated within the G-R model as

$$S(f) = 4egI_d. \quad (9)$$

It is valid in the range of electric fields and temperatures where statistical correlations between the elementary trapping-detrapping events from quantum dots are negligible. At low temperatures, where $\hbar\omega \gg k_B T$, the quantum zero-point fluctuations will play a dominant role than the thermal fluctuations. Therefore, at low temperature and low bias, the noise current appears to be proportional to the dark current and is essentially independent of frequency as shown in Figs. 2(a) and 2(b). Hence, thermally activated G-R processes from the quantum dots are negligible at low

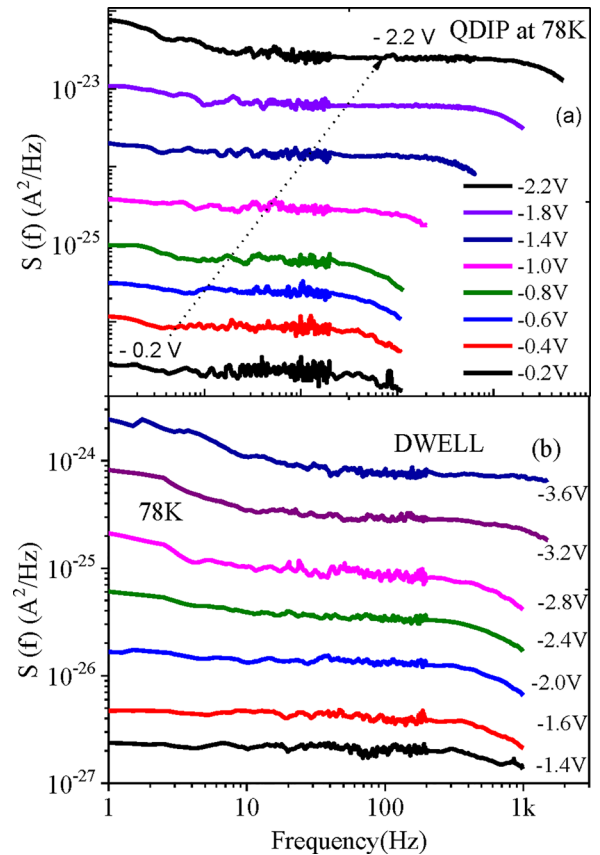


FIG. 2. Noise power spectral densities of QDIP (a) and DWELL (b) at 78 K for different biases. Both structures display similar noise behavior except the DWELL has lower power spectral density below the noise floor of noise measurement set up for bias voltage below -1.4 V. These noise spectral densities exhibit a linear dependence with external bias voltage, that is, shot (G-R) noise. The decreasing tendency of noise spectral density at the highest measurable frequency is due to the bandwidth limitation of low-noise pre-amplifier.

temperature. As a result, the G-R noise, which is characterized by random fluctuations in the current density, is the dominant noise source for QD-based detectors.¹¹ However, as the temperature increases from ~ 100 K to 130 K, in addition to the G-R noise, the $1/f$ noise current at lower frequencies and thermal noise currents have significant contributions to the noise power spectral density of QDIP as shown in Fig. 3. The noise spectral density has generally a form $S(f) = \frac{A}{f} + 4qI_{dg} \left(\frac{1}{1+(f/f_c)^2} \right) + \frac{4kT}{R}$, where f_c is the cut-off frequency for G-R noise. The theoretical fits in Fig. 3 show the cut-off frequencies beyond the band width of experimental measurements. These theoretical fits enable us to predict the cut-off frequency for G-R noise, and as the temperature decreases from 130 K to 90 K, the cut-off frequency decreases from 2.03×10^6 Hz to 1.45×10^5 Hz as shown by arrow in Fig. 3.

To get further insights into the device capture or relaxation properties, we measured the noise power spectral density, $S(f)$, which is nearly proportional to the dark current. Then, we extract the gain by calculating the G-R noise as per Eq. (8). The band width of measurement is limited by low-noise pre-amplifier gain that rolls off at higher frequencies. The gain roll-off frequency depends on the impedance to be measured. Therefore, at low bias and low temperature, where impedance of devices is as high as ~ 1 – 10 M-ohm, the band width of the measurement is limited to a frequency of ~ 100 Hz as shown in Fig. 2. However, for low impedance condition (high temperature and high bias), up to 100 kHz band width is measured as shown in Fig. 3.

B. Carrier scattering in heterostructures and QD-based detectors

The carrier scattering or capture probability determines the responsivity through the photoconductive gain. In a typical semiconductor, the electrons and holes scatter via longitudinal optical (LO) phonon and longitudinal acoustic (LA)

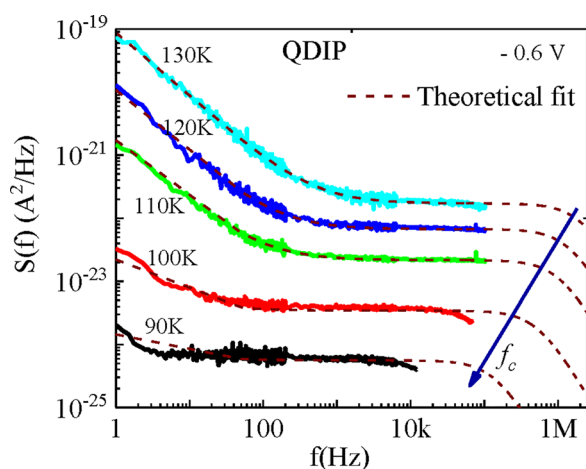


FIG. 3. Noise power spectral density of QDIP at -0.6 V and different temperatures. As the temperature increases, $1/f$ noise at lower frequency and thermal noise currents will have significant contributions to the noise power spectral density. Similar behavior was seen for DWELL which is not shown here. The dash lines represent the theoretical fits. The arrow shows theoretically fitted cut-off frequency of frequency f_c for G-R noise which decreases with temperature.

phonon emission. But the LO phonons are highly monochromatic (~ 30 meV in InAs, ~ 36 meV in GaAs, and ~ 46 meV in AlAs).²⁶ Thus, the carrier relaxation probability through LO phonon scattering is largely reduced in QD structures due to discrete energy levels, and the carrier's relaxation time from excited states increases. Acoustic phonon scattering is also reduced because of the conservation of both energy and momentum between discrete energy levels within a QD. (The LA phonon energy is 3 meV when the wavelength of the acoustic phonon is of approximately the QD diameter.) In GaAs/AlGaAs heterostructures where there is no energy confinement, both LO and LA phonon emissions cannot be ruled out. Hence, the key advantage of QD-based devices is the longer carrier relaxation time due to the existence of discrete energy levels that hamper phonon assisted carrier scattering,^{26,27} the so-called “phonon bottleneck”. Experimental results showed that carriers within heterostructures relax much faster than that in QDs and consequently have lower gain. Figure 4 shows a comparison of measured dark current gains between QD-based structures and GaAs/Al_{0.28}Ga_{0.72}As heterostructure. Due to the suppression of phonon scattering mechanism in QD structures, carriers in both QDIP and DWELL have higher life time as compared to the heterostructure with reasonably the same response wave length range, ~ 2 μ m– 10 μ m. Thus, the experimentally measured gain of QDIP and DWELL is significantly larger than that of GaAs/Al_{0.28}Ga_{0.72}As (Fig. 4).

C. Gain and capture probability

Important characteristics of QD-based IR detectors are determined almost entirely by the photo-generation rate of carriers out of the QDs and the recapture (or capture probability) into the QDs. The capture probability (p_c) determines the responsivity through the photoconductive gain. The gain and hole capture probability can thus be calculated using Eqs. (7) and (8). Figure 5(a) shows an experimentally

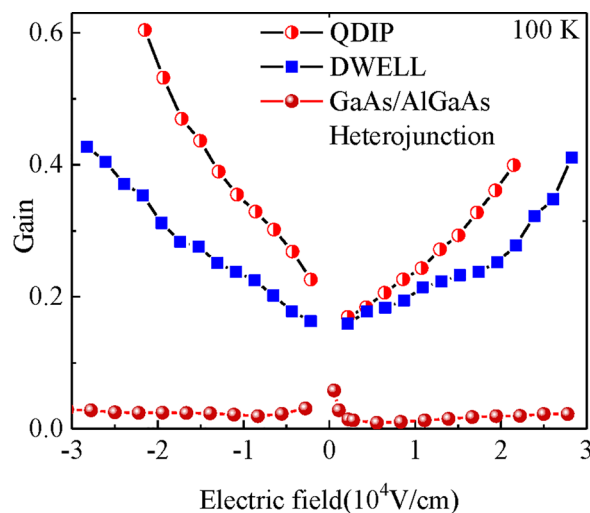


FIG. 4. Comparison of experimentally measured gain between QD structures and GaAs/Al_{0.28}Ga_{0.72}As heterostructure. Since the phonon scattering mechanism is reduced in QD structures, both QDIP and DWELL exhibit higher gain as compared to GaAs/Al_{0.28}Ga_{0.72}As heterostructure due to longer carriers' life time.

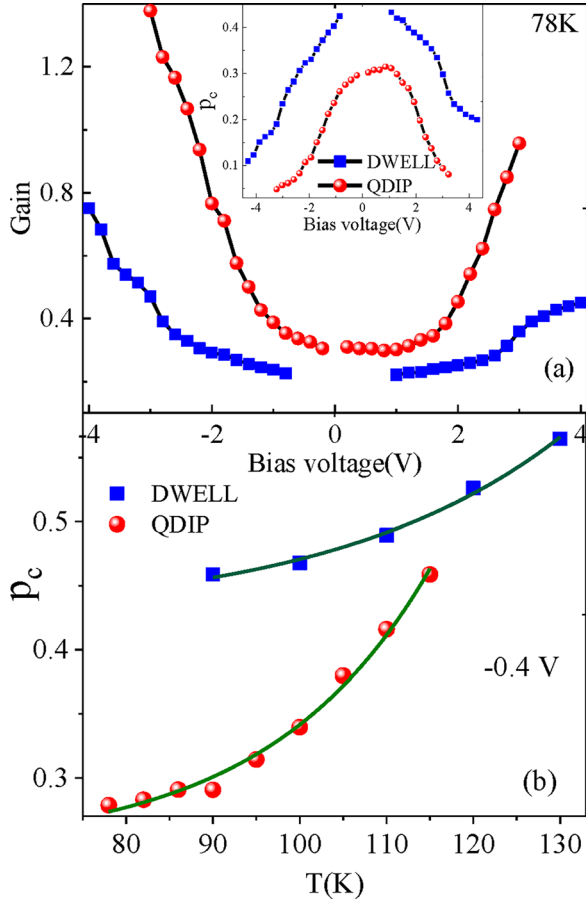


FIG. 5. (a) Comparison of gain between QDIP and DWELL. QDIP has higher gain values as compared to DWELL. The inset shows DWELL has higher capture probability (p_c) than the corresponding QDIP. (b) Experimentally measured capture probability (■ and ● lines) of holes at bias voltage -0.4 V and different temperatures. The solid line is the exponential fits of capture probabilities of QDIP and DWELL. Hence, the capture probability increases exponentially with temperature.

measured gain comparison between QDIP and DWELL. The gain values of QDIP are higher than the corresponding DWELL sample. DWELL has additional confinements in the well that results in additional transitions between bound to bound which has higher capture probability as compared to transition between bound to quasi-bound or continuum. Thus, DWELL has about two times higher capture probability than the corresponding QDIP as shown in Fig. 5(a) inset. As indicated in Fig. 5(b), p_c slightly increases as the temperature increases. Although the total number of states remains constant, due to thermal emission, the unoccupied hole states in the QDs likely increase with the temperature, and hence, p_c increases with a rate proportional to $e^{E_i/KT}$. The capture probability can also be defined as $p_c = \frac{\tau_t}{\tau_{rec}}$, where τ_t is the sweep-out or transit time and τ_{rec} is the recombination time (lifetime). The transit time is given by^{28,29}

$$\tau_t = h_{QD} \frac{\sqrt{1 + \left(\frac{\mu F}{v_s}\right)^2}}{\mu F}, \quad (10)$$

where h_{QD} is the QD height and v_s is the saturation velocity of holes. The recombination (lifetime) is²⁹

$$\tau_{rec} = \frac{(N+1)L}{\pi a_{QD}^2 h_{QD} \Sigma_{QD} V_t}, \quad (11)$$

where N is the number of QD layers, a_{QD} is the lateral dimension of QD, L is the spacing between the QD layers, Σ_{QD} is the surface density of QDs, and V_t is the capture rate of holes. In the case when $\tau_t \ll \tau_{rec}$, the capture probability p_c is low, and the gain has the conventional expression as

$$g = \frac{\tau_{rec}}{N\tau_t} = \frac{(N+1)L\mu F}{N\pi a_{QD}^2 h_{QD}^2 \Sigma_{QD} V_t \left(1 + \left(\frac{\mu F}{v_s}\right)^2\right)^{1/2}}. \quad (12)$$

Based on Eq. (12), it is possible to see that optimizing the structural parameters, such as the QD density Σ_{QD} , barrier thickness L , number of QD layers N , QDs, and barrier materials, and tuning the bias voltage $F(V)$ leads to minimize the capture probability and improve the gain of QDIP and DWELL. The capture probability (p_c) versus gain for QDIP and DWELL for bias voltages from -3.0 V to 3.0 V is shown in Fig. 6. For QDIP, a maximum gain of 1.4 was obtained at -3.0 V with a capture probability (least) of 0.05 and a minimum gain of 0.31 was obtained at $+0.2$ V with a capture probability of 0.3. Similarly, DWELL's gain follows the same variation with capture probability except DWELL has lower gain values as compared to the corresponding QDIP as expected. Since both gain and capture probability are expressed in terms of material and structural parameters in Eqs. (11) and (12), it is possible to optimize the device for higher gain (the responsivity, $\mathcal{R} \propto g$). Hence, material with high mobility, number of QD layers with optimized total thickness, and thickness of barrier (80 nm for GaAs) are some of the parameters that improve device performance.

Combination of Eqs. (5), (9), and (12) yields the expression for noise power spectral density as

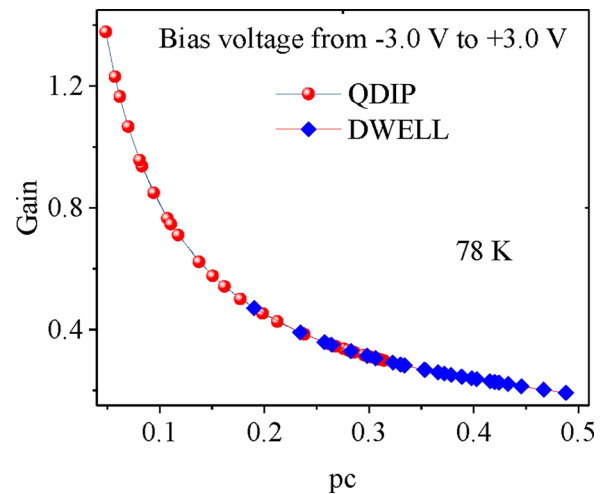


FIG. 6. The capture probability (p_c) versus gain for QDIP and DWELL for bias voltages from -3.0 V to 3.0 V. For QDIP, a maximum gain of 1.4 was obtained at -3.0 V with the least capture probability of 0.05 and a minimum gain of 0.31 was obtained at $+0.2$ V with a capture probability of 0.3. Similarly, DWELL's gain follows the same variation with capture probability except DWELL has lower gain values as compared to the corresponding QDIP.

TABLE II. Fitting parameters for noise power spectral density of DWELL and QDIP at 77 K.

	DWELL		QDIP	
	-ve bias	+ve bias	-ve bias	+ve bias
μ (cm ² /V s)	215	95	246	217
V_s (10 ⁶ cm/s)	1.43	1.35	2.27	2.25
V_t (10 ⁵ s ⁻¹ m)	200	195	2.98	2.40
β (m C)	1.98	2.45	3.01	3.58

 $S(V)$

$$= \frac{8e^2 \mu^2 F^2(V) (N+1) LA \left(\frac{m^* kT}{2\pi \hbar^2} \right)^{3/2} \exp\left(-\frac{E_0 - \beta F(V)}{kT} \right)}{N\pi a_{QD}^2 h_{QD}^2 \Sigma_{QD} V_t \left(1 + \left(\frac{\mu F(V)}{v_s} \right)^2 \right)^{1/2}} \quad (13)$$

Theoretical expression for noise power spectral density for both negative positive bias regions fits well to the experimental data with fitting parameters in Table II, as shown in Fig. 7. The fitting parameters of the dark current density in Fig. 1(b) and the corresponding negative bias noise power spectral density in Fig. 7 are nearly the same. The differences in the fitting parameters for the negative (-ve) and positive (+ve) biases are due to the asymmetry in the structures. Since both devices have lower resistance for negative bias as compared to that of corresponding positive bias, the negative bias V_s and μ are higher than the corresponding positive bias. Furthermore, theoretical fit to the noise power spectral density reveals that the capture rate of DWELL is higher than the corresponding QDIP which agrees with the capture probabilities [inset of Fig. 5(a)] obtained from experimentally measured gain. However, DWELL architecture offers additional advantages over QDIP detectors, such as superior optical

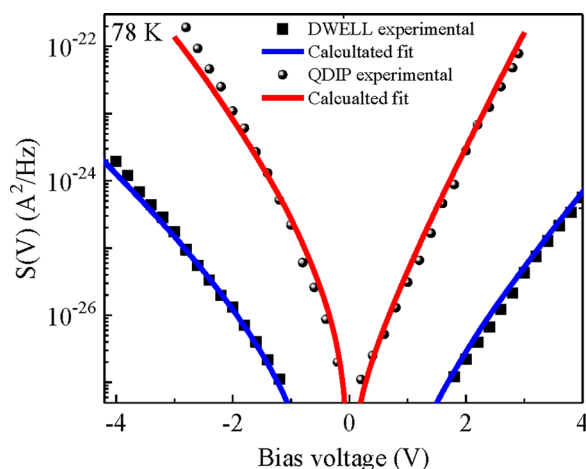


FIG. 7. Theoretical fits to the experimental data for both QDIP and DWELL samples. The constant parameters are $N=10$, $L=80$ nm, $a_{QD}=20$ nm, $h_{QD}=5$ nm, $\Sigma_{QD}=5 \times 10^{10}$ cm⁻², and $E_0=0.254$ eV. See Table II for the fitting parameters. The fitting parameters of the dark current density [Fig. 1(b)] and the noise power spectral density (Fig. 7) are nearly the same in each of the structures.

quality of the quantum dots due to strain relaxation^{30,31} in the InGaAs QW, and the ability to independently control the ground state and excited state energy in obtaining the bound to quasi-bound transitions for optimizing the capture probability. Additionally, the optimized bound-quasibound transition-based device can be further improved by the introduction of confinement enhancing barriers, such as resonant tunneling barriers around the DWELL region,²¹ which selectively block the dark current while allowing the photocurrents of the desired wavelengths to pass. This implies that the asset of DWELL structures deserves further research on the relevant carrier capture and relaxation mechanisms to improve the gain.

IV. CONCLUSION

The noise power spectral densities of DWELL and QDIP are experimentally determined. At lower temperature (below ~ 100 K) and low bias, the noise current of these devices is dominated by generation-recombination (G-R) noise. The noise gain, capture probability, and carriers' life time for bound-to-continuum or quasi-bound transitions in both DWELL and QDIP structures are discussed. The capture probability of DWELL is found to be more than two times higher than the corresponding QDIP. Based on the analysis, structural parameters such as the numbers of active layers, the surface density of QDs, and the carrier capture or relaxation rate, type of material, and electric field are some of the optimization parameters identified to improve the photoconductive gain of devices.

ACKNOWLEDGMENTS

This work was supported in part by the U.S. National Science Foundation and the U.S. Army Research Office under Grant Nos. ECCS-1232184 and W911 NF-15-1-0018, respectively. The Shanghai group acknowledges supports from the Natural Science Foundation of China (91221201). Financial support provided by The Center for Diagnostics and Therapeutics to Fellowship of Georgia State University, Atlanta, Georgia, USA, is also acknowledged.

¹G. Huang, J. Yang, P. Bhattacharya, G. Ariyawansa, and A. G. U. Perera, *Appl. Phys. Lett.* **92**, 011117 (2008).

²S. Adhikary, Y. Aytac, S. Meesala, S. Wolde, A. G. U. Perera, and S. Chakrabarti, *Appl. Phys. Lett.* **101**, 261114 (2012).

³M. R. Matthews, R. J. Steed, M. D. Frogley, C. C. Phillips, R. S. Attaluri, and S. Krishna, *Appl. Phys. Lett.* **90**, 103519 (2007).

⁴V. Ryzhii, *Semicond. Sci. Technol.* **11**, 759 (1996).

⁵B. Kochman, A. D. Stiff-Roberts, S. Chakrabarti, J. D. Phillips, S. Krishna, J. Singh, and P. Bhattacharya, *IEEE J. Quantum Electron.* **39**, 459 (2003).

⁶A. Stiff-Roberts, S. Krishna, P. Bhattacharya, and S. Kennerly, *J. Vac. Sci. Technol. B* **20**, 1185 (2002).

⁷A. Marent, T. Nowozin, J. Gelze, F. Luckert, and D. Bimberg, *Appl. Phys. Lett.* **95**, 242114 (2009).

⁸D. Pan, E. Towe, and S. Kennerly, *Appl. Phys. Lett.* **75**, 2719 (1999).

⁹A. D. Stiff, S. Krishna, P. Bhattacharya, and S. Kennerly, *Appl. Phys. Lett.* **79**, 421 (2001).

¹⁰S. Raghavan, P. Rotella, A. Stintz, B. Fuchs, S. Krishna, C. Morath, D. A. Cardimona, and S. W. Kennerly, *Appl. Phys. Lett.* **81**, 1369 (2002).

¹¹Z. Ye, J. C. Campbell, Z. Chen, E.-T. Kim, and A. Madhukar, *Appl. Phys. Lett.* **83**, 1234 (2003).

¹²B. F. Levine, *J. Appl. Phys.* **74**, R1-R81 (1993).

- ¹³A. I. Yakimov, V. V. Kirienko, V. A. Armbrister, A. A. Bloshkin, and A. V. Dvurechenskii, *Appl. Phys. Lett.* **107**, 213502 (2015).
- ¹⁴Y.-F. Lao, S. Wolde, A. G. U. Perera, Y. H. Zhang, T. M. Wang, H. C. Liu, J. O. Kim, T. Schuler-Sandy, Z.-B. Tian, and S. S. Krishna, *Appl. Phys. Lett.* **103**, 241115 (2013).
- ¹⁵Y.-F. Lao, S. Wolde, A. G. U. Perera, Y. H. Zhang, T. M. Wang, J. O. Kim, T. Schuler-Sandy, Z.-B. Tian, and S. S. Krishna, *Appl. Phys. Lett.* **104**, 171113 (2014).
- ¹⁶Y. F. Lao, P. K. D. D. P. Pitigala, A. G. U. Perera, H. C. Liu, M. Buchanan, Z. R. Wasilewski, K. K. Choi, and P. Wijewarnasuriya, *Appl. Phys. Lett.* **97**, 091104 (2010).
- ¹⁷H. C. Liu, *Opto-Electronics Review* **11**(1), 1–5 (2003).
- ¹⁸V. Mitin, *Phys. Rev. B* **31**, 2584 (1985).
- ¹⁹H. Liu and J. Zhang, *Opt. Laser Technol.* **44**, 1536 (2012).
- ²⁰L. Lin, H. L. Zhen, N. Li, W. Lu, Q. C. Weng, D. Y. Xiong, and F. Q. Liu, *Appl. Phys. Lett.* **97**, 193511 (2010).
- ²¹X. Su, S. Chakrabarti, P. Bhattacharya, G. Ariyawansa, and A. G. U. Perera, *IEEE J. Quantum Electron.* **41**, 974 (2005).
- ²²M. Sotoodeh, A. Khalid, and A. Rezazadeh, *J. Appl. Phys.* **87**, 2890 (2000).
- ²³R. Quay, C. Moglestue, V. Palankovski, and S. Selberherr, *Mater. Sci. Semicond. Process.* **3**, 149 (2000).
- ²⁴A. Delga, L. Doyennette, M. Carras, V. Trinité, and P. Bois, *Appl. Phys. Lett.* **102**, 163507 (2013).
- ²⁵W. A. Beck, *Appl. Phys. Lett.* **63**, 3589 (1993).
- ²⁶H. Benisty, C. M. Sotomayor-Torrès, and C. Weisbuch, *Phys. Rev. B* **44**, 10945 (1991).
- ²⁷J. Urayama, T. B. Norris, J. Singh, and P. Bhattacharya, *Phys. Rev. Lett.* **86**, 4930 (2001).
- ²⁸H. Liu and J. Zhang, *Appl. Opt.* **51**, 2767 (2012).
- ²⁹A. Mahmoodi, H. D. Jahromi, and M. H. Sheikhi, *IEEE Sens. J.* **15**, 5504 (2015).
- ³⁰A. Stintz, G. Liu, A. Gray, R. Spillers, S. Delgado, and K. Malloy, *J. Vac. Sci. Technol. B* **18**, 1496 (2000).
- ³¹Z. Ye, J. C. Campbell, Z. Chen, E.-T. Kim, and A. Madhukar, *J. Appl. Phys.* **92**, 7462 (2002).